Send Orders for Reprints to reprints@benthamscience.ae

622 *Letters in Drug Design & Discovery,* 2015, *12,* 622-627

Substrate – Inositol Transporter Interactions: Molecular Docking Study

Mariyana Atanasova and Irini Doytchinova*

Faculty of Pharmacy, Medical University of Sofia, 2 Dunav st., Sofia 1000, Bulgaria

Irini Doytchinova

Abstract: Inositol is a cyclic polyol naturally occurring as seven optically inactive stereoisomers and one enantiomeric pair. Within the human body, brain is the most saturated organ of inositol, mainly with myo- and scyllo-inositol. One of the molecular mechanisms for the maintenance of inositol brain levels is active transport via stereospecific carrier molecules – one hydrogen myo-inositol transporter (HMIT) and two sodium myo-inositol transporters (SMIT1 and SMIT2). In this study, we modeled by homology the myo-inositol transporter SMIT1 using the X-ray structure of Vibrio parahaemolyticus sodium/galactose symporter (vSGLT) as a template. A set of inositol derivatives – strong and weak competitors of inositol transport – was docked in the SMIT1 binding site. The docking protocol was optimized in terms of scoring function, radius of the binding site and flexible residues inside to distinguish between strong and weak competitors. The analysis of ligand – transporter interactions revealed that tiny structural differences exist between strong and weak competitors. Both groups have almost equal number of hydroxyl groups but the strong competitors are able to form more hydrogen bonds with the transporter (5.07 *vs*. 4.53 per molecule) and take part in less hydrophobic interactions (0.6 vs. 0.73) than the weak competitors.

Keywords: Inositol, SMIT1, docking, strong and weak competitors, hydrogen bonds, hydrophobic interactions.

INTRODUCTION

Inositol is a cyclic polyol naturally occurring as seven optically inactive stereoisomers and one enantiomeric pair [1]. Commonly found in nature are *myo-, scyllo-, chiro-* and *epi*-inositol, whereas *myo*-Inositol is a component of all eukaryotic cells and is the most widespread isomer [1]. Within the human body, brain is the most saturated organ of inositol, mainly with *myo-* and *scyllo*-inositol [2,3]. Their concentration in the brain is about 100-fold greater than the circulating levels [1, 4]. Both isomers are endogenously found [2, 3]. Inositol in the body is formed mainly in kidneys, but brain, testis and liver also synthesize it [5,6]. In brain, inositol can be provided via in situ transformation of glucose only by endothelial cells and via entering through the blood-brain barrier and blood-CSF barrier. One of the molecular mechanisms for the maintenance of inositol brain levels is active transport via stereospecific carrier molecules – one hydrogen *myo*-inositol transporter (HMIT) and two sodium *myo*-inositol transporters (SMIT1 and SMIT2) [7-12].

Inositol is extensively studied as a therapeutic agent during the last decades. Preliminary studies showed effective treatment with *myo*-inositol in cases of psychiatric disorders such as depression, panic, obsessive compulsive disorder [13-19]. Recently, it has been found that *scyllo*-inositol successfully inhibits the growth of Aβ amyloid plaques and cognitive deficits in TgCRND8 mice which show many of the hallmark features of Alzheimer's disease (AD) [20, 21]. Currently *scyllo*-inositol is in human clinical trials for the treatment of AD [22].

*Address correspondence to this author at the Faculty of Pharmacy, Medical University of Sofia, 2 Dunav st., Sofia 1000, Bulgaria;
Tel: +359 2 9236506. Fax: +359 2 9879874;
Email: idoytchinova@pharmfac.net

Inositol transporters belong to the family of Solute Sodium Symporters (SSS, TC 2.A.21) which cotransport Na^+ with sugars, amino acids, inorganic ions, vitamins, *myo*-inositol, phenyl acetate, urea and water [23]. The members of this family consist of 11 to 15 transmembrane domains in α-helical conformation arranged around of a large cavity with extra- and intracellular hydrophobic gates [24]. The solute and Na^+ are bound in the center of this cavity. During the transport process, the carrier passes through several conformational states [25]. Initially, the transporter free of substrate and Na^+ resides in a closed state. Na^+ binding turns the transporter to outward-open conformation and opens the substrate-binding site. The substrate binds to its site and this in turn closes the external gate, without changes to the external vestibule (outward-occluded state). The next step involves the closure of the external vestibule to form a fully occluded state. The substrate release begins with exposure of the substrate vestibule to the intracellular environment (inward-occluded state). Once Na^+ is released, the internal gate opens to permit substrate release (inward-open state). Finally, the internal vestibule closes and the transporter returns to its initial unbound state. According to White's classification of membrane proteins of known 3D structure [26], the SSS family is presented in Protein Data Bank [27] by only one X-ray structure – the *Vibrio parahaemolyticus* sodium/galactose symporter (vSGLT, pdb code: 3DH4) [28]. In this structure, the symporter is in an inward-facing conformation with the substrate bound inside the cavity. This conformation is quite appropriate for docking studies as it locates the substrate binding site and indicates the substrate bound conformation.

In this study, we modeled by homology the *myo*-inositol transporter SMIT1 using the X-ray structure of vSGLT as a template. A set of inositol derivatives – strong and weak competitors of inositol – was docked in the SMIT1 binding

1875-628X/15 $58.00+.00

site and the docking protocol was optimized to distinguish between them. The modeled complexes revealed the main structural features responsible for the substrate – transporter interactions.

MATERIALS AND METHODS

Homology Modeling of Myo-inositol Transporter SMIT1

The *myo*-inositol transporter SMIT1 was modeled by homology using the SWISS-MODEL tool of the ExPASy web server [29]. The SMIT1 sequence (uniprot code: P53794) was input as a target sequence and the X-ray structure of vSGLT (pdb code: 3DH4) was uploaded as a template. As the vSGLT structure was a homo-tetramer, the modeled SMIT1 structure was also consisted of four identical monomers. Only one monomer (chain A) was used in the docking simulations. The geometry of modelled monomer protein was optimized by OPLS (Optimized Potentials for Liquid Simulations) molecular field at the following settings: dielectric constant 78; 0.5 and 0.125 scale factors for electrostatic and van der Waals interactions, respectively; steepest descent algorithm with RMS gradient of 0.1 kcal/Åmol. The optimized geometry was subjected to MD simulation in water at 310ºK for 1 ns using YASARA force field [30].

Dataset of SMIT1 Substrates

A set of 30 SMIT1/2 ligands was collected from the literature [31] and used in the docking studies. The set consisted of 15 inositol isomers, 6 hexoses, 2 pentose sugars and 7 *scyllo*-inositol derivatives which may serve as competitive substrates, inhibitors or allosteric effectors in inositol transport. The structures are given as Appendix 1. Originally, the *myo*-inositol-(2-^{3}H) and *scyllo*-inositol-(2-^{3}H) transports were tested in the presence or absence of these compounds and it was found that *myo*-inositol, *scyllo*-inositol, D-*chiro*-inositol, D-pinitol, viburnitol, sequoyitol, D-ononitol, D-glucose, D-mannose, L-fucose, 1-O-methyl-*scyllo*-inositol, 1-chloro-1-deoxy-*scyllo*-inositol, 1-fluoro-1-deoxy-*scyllo*-inositol, 1-azide-1-deoxy-*scyllo*-inositol and 1-deoxy-*scyllo*-inositol significantly depressed the transport. At concentrations of 10 mM, they decreased the [^{3}H]*myo*-inositol counts per minute (cpm) up to 12,000. These molecules were defined as SMIT1 strong competitors. The remaining compounds were defined as weak competitors. We assume that all the compounds that were tested bind in approximately the same area of the transporter and that allosteric modulators would not be identified by the approach reported in this manuscript.

Molecular Docking Protocol

The molecular docking was performed by GOLD v. 5.1 (CCDC) [32]. The docking protocol was optimized in terms of scoring functions, radius of the binding site and flexible amino acids in the binding site. No water molecules exist in the substrate binding site. Four scoring functions were assessed: ChemPLP, ChemScore, GoldScore and ASP. Five radii of the binding site (6Å to 10Å) and up to 10 flexible amino acids inside were tested. Each run generated 50 docking poses. The poses were ranked according to the highest fitness score. Each docking run was repeated three times and the average fitness score was considered. At each step, the goodness of docking was assessed by the ratio (*R*) between the average scores of strong and weak competitors. As higher is the *R* value as better the docking protocol distinguishes between strong and weak competitors.

Visualization

The interactions between the ligands and SMIT1 protein were visualized by YASARA v.12.11.25 [30]. Two types of interactions were considered: hydrogen bonds and hydrophobic interactions. For visualizing of hydrogen bonds, an extended selection was used to include all hydrogen bonding partners of the bound ligand. The hydrophobic interactions are shown at distances below 5.0 Å.

RESULTS AND DISCUSSION

The X-ray structure of *Vibrio parahaemolyticus* sodium/galactose symporter (vSGLT, pdb code: 3DH4) was used as a template for the homology modeling of *myo*-inositol transporter SMIT1. The template is a homo-tetramer but the transporter proteins function as monomers. Thus, only chain A was used in the modeling. The modeled SMIT1 had 39.86% sequence identity within the range 42 – 533 residues with the template. The GMQE and QMEAN4 scores were 0.57 and -13.97, respectively. Although the negative QMEAN4 global score, the substrate binding site had positive local scores (Appendix 2) allowing to use the modeled protein in docking simulations. Additionally, the geometry of the modeled protein was optimized by MD simulations for 1 ns and the RMSD was 7.141Å over 3797 matched non-hydrogen atoms. The RMSD values for the gates residues Leu68, Trp82, Tyr275 and Tyr438 were 0Å. Ramachardan plot is provided as Appendix 3. Similarly to vSGLT, the modeled protein consists of 14 membrane spanning helices (TM) with extracellular amino- and carboxy-termini. The structural core is formed from inverted repeats of 5 TM helices (TM2-TM6 and TM7-TM11) placing it in an inward facing conformation. The extracellular gate in SMIT1 is formed by residues Leu68, Trp82 and Tyr438 which corresponds to Met73, Tyr87 and Phe424 in vSGLT [28] (Fig. **1**). The intracellular gate is shaped by one residue

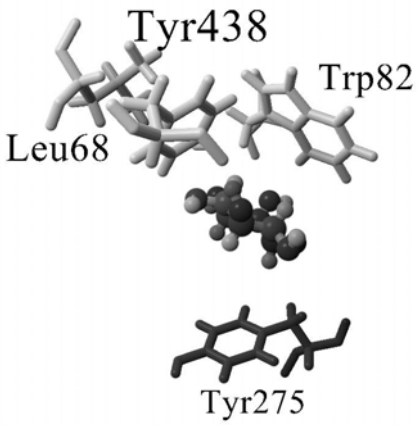

Fig. (1). Complex of *myo*-inositol and modeled SMIT1; External gate residues (in gray), internal gate residues (in black) and bound *myo*-inositol (in ball-and-stick) are shown.

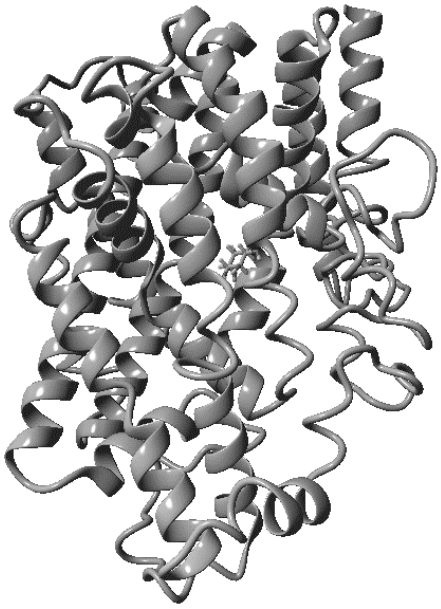

Fig. (2). Complex of *myo*-inositol and modeled SMIT1; Protein is given as ribbon, substrate – as sticks.

Table 1. The ratio *R* between the average fitness scores of strong and weak competitors when different scoring functions are used.

Scoring Function	ChemPLP	ChemScore	GoldScore	ASP
R	0.989	1.026	0.985	1.014

Table 2. The ratio *R* between the average fitness scores of strong and weak competitors at different radii of the binding site.

Radius, Å	6	7	8	9	10
ChemScore	0.926	1.034	1.035	1.026	1.018
ASP	1.018	1.012	1.020	1.014	1.011

– Y275 corresponding to Y263 in vSGLT [28]. *myo*-Inositol, by analogy to galactose, was docked in the center of the core using the same coordinates. The modeled structure of SMIT1 with docked *myo*-inositol is shown in (Fig. **2**).

The set of 30 SMIT1/2 ligands consists of 15 strong and 15 weak competitors. The ligands were docked in the modeled SMIT1 and the protocol was optimized stepwise. The ratio *R* between the average scores of strong and weak competitors was used as a criterion for the goodness of docking. Initially, the protocol was optimized in terms of scoring function. Four scoring functions as implemented in GOLD were tested: ChemPLP, ChemScore, GoldScore and ASP. The docking was performed at the following settings: rigid protein, flexible ligand, radius of binding site 9Å. The *R* values are given in Table **1**.

Two scoring functions, ChemScore and ASP, gave slightly higher scores for the strong competitors than for the weak ones ($R > 1$). Next, both of them were used to optimize the docking protocol in terms of the radius of the binding site. Five radii were tested – from 6Å to 10Å – at rigid protein and flexible ligand. The *R* values are given in Table **2**. It is evident that ChemScore distinguishes better between strong and weak competitors than ASP at 7Å – 10Å. These settings were used further in the docking optimization.

Table 3. The ratio *R* between the average fitness scores of strong and weak competitors at different radii of the binding site and flexible amino acids; Leu68, Trp82, Tyr275 and Tyr438.

Radius, Å	7	8	9
ChemScore	1.040	1.028	1.030
ASP	0.990	1.000	0.990

Table 4. The ratio *R* between the average fitness scores of strong and weak competitors applying ChemScore at 9Å and different combinations of flexible residues in the binding site.

Radius, Å	Flexible residues in the binding site	R
9	Leu68, Trp82, Tyr275, Tyr438, Asn85	1.069
9	Leu68, Trp82, Tyr275, Tyr438, Arg252	1.077
9	Leu68, Trp82, Tyr275, Tyr438, Arg252, Asn85	1.209
9	Leu68, Trp82, Tyr275, Tyr438, Arg252, Asp446	1.211
9	Leu68, Trp82, Tyr275, Tyr438, Asn85, Thr269	1.533
9	Leu68, Trp82, Tyr275, Tyr438, Arg252, Asn85, Trp276	1.504
9	Leu68, Trp82, Tyr275, Tyr438, Arg252, Asp446, Phe505	1.423
9	Leu68, Trp82, Tyr275, Tyr438, Asn85, Thr269, Trp276	2.190

At the final step, the docking protocol was optimized in terms of the number and position of flexible amino acids in the binding site. The initial set of flexible amino acids contains only those forming the extra- and intracellular gates of the transporter: residues Leu68, Trp82, Tyr275 and Tyr438 (Fig. **1**). The flexibility of these residues changes the *R* values. The *R* values for ASP decreased and this scoring function was not considered further in the optimization. The *R* values for ChemScore slightly decreased at 8Å but increased at 7Å and 9Å (Table **3**).

Apart from these four residues forming the gates, the ligands make contacts with several other residues from the binding site. The effect of flexibility of these additional residues on the discrimination between strong and weak competitors was tested gradually applying ChemScore at 7Å, 8Å and 9Å at different combinations of flexible residues in the binding site. The best combinations are given in Table **4**.

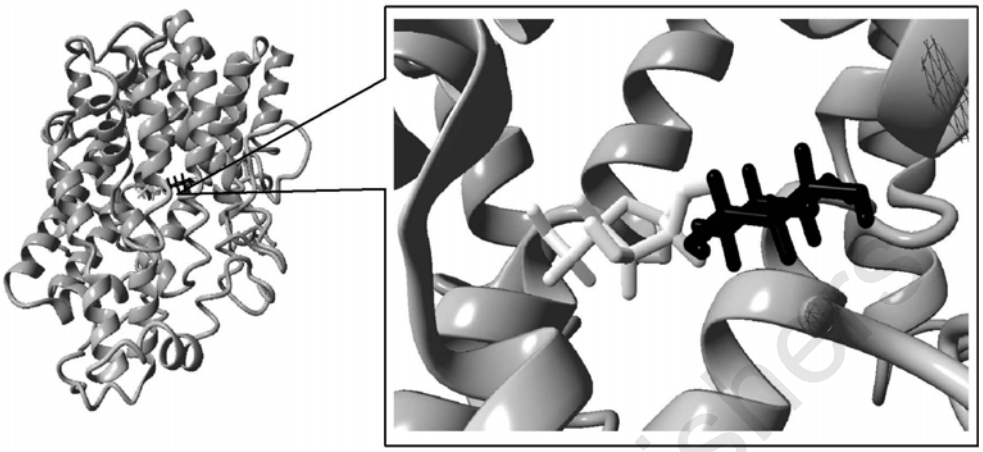

Fig. (3). Superposed 1-deoxy-*scyllo*-inositol – SMIT1 and L-ribose – SMIT1 complexes. The strong (white) and the weak competitor (black) take close but non-overlapping positions.

All of the best combinations of flexible residues operate in a binding site with 9Å radius. The highest value of 2.190 for *R* was achieved when the following residues were flexible: Leu68, Trp82, Tyr275, Tyr438, Asn85, Thr269 and Trp276. Further addition of flexible residues decreases *R* (data not shown). The combinations of flexible residues in binding sites with 7Å and 8Å give lower values for *R*. In short, the final settings of the optimized docking protocol used to discriminate between strong and weak inositol competitors were: scoring function ChemScore, radius of the binding site 9Å, flexible ligand and seven flexible residues in the binding site as listed above. At these settings, the strong competitors show an average score two times higher than the average score of the weak competitors.

To analyze the interactions between ligands and SMIT1 protein, each complex was visualized in YASARA. As the inositol competitors are polyols containing different number of methyl groups, only two types of interactions were considered – hydrogen bonds and hydrophobic interactions. The average hydroxyl groups are 5.13 per molecule for the strong competitors and they form 5.07 hydrogen bonds in average, while the average hydroxyl groups for the weak competitors are 4.93 per molecule and they form 4.53 hydrogen bonds in average. The weak competitors are not able to implement all their hydroxyl groups into hydrogen bonds with the transporter. Additionally, the average hydrophobic interactions per molecule are 0.60 for the strong and 0.73 for the weak competitors at almost the same number of methyl groups. These tiny differences between weak and strong competitors indicate that SMIT1 is very sensitive to even small changes in ligand structure. Substrate transport of labeled *myo*- and *scyllo*-inositol showed that the transport of scyllo-inositol is substantially slower despite the recognition of both substances with similar affinity [31].

The main SMIT1 residues involved in the hydrogen bond formations are Gln59, Glu63, Trp82, Glu83, Tyr438 and Gln442 (Fig. **1**). Tyr438 and Gln442 interact with the ligand hydroxyl groups at C1 and C2; Gln59, Glu63 and Glu83 interact with the hydroxyl groups at C3, C4 and C5. Additionally, Trp82 and Ser272 form hydrogen bonds with D-ononitol, and Asn85 interacts with D-pinitol. The complexes with the highest and lowest ChemScores are superposed in (Fig. **3**). The former complex is 1-deoxy-*scyllo*-inositol – SMIT1 and the latter – L-ribose – SMIT1. The ligand 1-deoxy-*scyllo*-inositol is a strong competitor, L-ribose – a weak competitor. The competitors take close but non-overlapping positions.

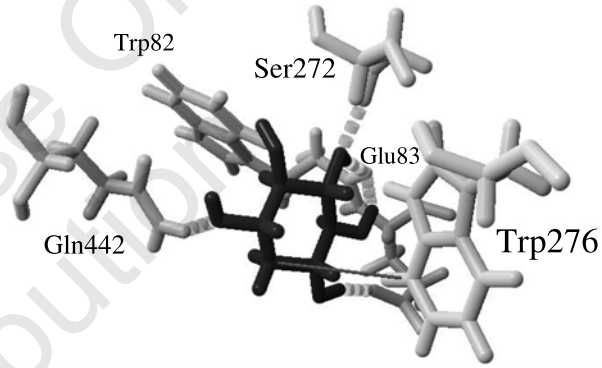

Fig. (4). The strong competitor 1-deoxy-*scyllo*-inositol (black) takes part in five hydrogen bonds with Trp82, Glu83, Ser272 and Gln442 (dotted lines) and in one hydrophobic interaction with Trp276 (gray line).

The strong competitor 1-deoxy-*scyllo*-inositol takes part in five hydrogen bonds with Trp82, Glu83, Ser272 and Gln442 and in one hydrophobic interaction with Trp276 (Fig. **4**). The weak competitor *L*-ribose forms four hydrogen bonds with Asn59 and Glu63 and one hydrophobic interaction with His64 (Fig. **5**).

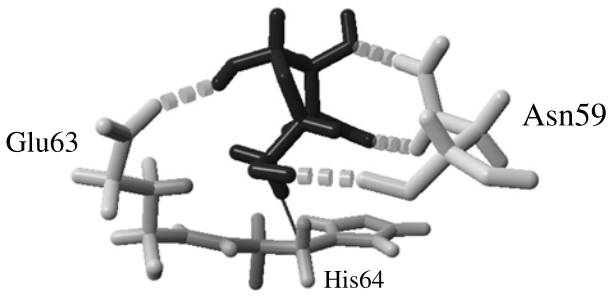

Fig. (5). The weak competitor *L*-ribose (black) forms four hydrogen bonds with Asn59 and Glu63 (dotted lines) and one hydrophobic interaction with His64 (gray line).

In short, the strong competitors are able to form more hydrogen bonds with the transporter (5.07 *vs.* 4.53) and take part in less hydrophobic interactions (0.6 *vs.* 0.73) than the weak competitors. The strong and weak competitors take close but non-overlapping positions in the transporter binding site. These tiny structural differences in closely related inositol derivatives strongly affect the substrate – SMIT1 interactions.

CONCLUSION

The structure of *myo*-inositol transporter SMIT1 was modeled by homology for the first time using the X-ray structure of *Vibrio parahaemolyticus* sodium/galactose symporter (vSGLT) as a template. A stepwise docking protocol was developed to dock a set of inositol derivatives transported by SMIT1. The protocol was optimized to discriminate between strong and weak inositol competitors. The modeled complexes revealed that the strong competitors make more hydrogen bonds with the protein than the weak ones at almost equal number of hydroxyl groups per molecule. Additionally, the strong competitors are involved into less hydrophobic interactions with SMIT1 than the weak competitors at almost the same number of methyl groups per molecule.

CONFLICT OF INTEREST

The authors confirm that this article content has no conflict of interest.

ACKNOWLEDGEMENTS

The present research was supported by the National Research Fund, Ministry of Education and Science, Bulgaria, Grant 02-1/2009.

SUPPLEMENTARY MATERIAL

Supplementary material is available on the publisher's web site along with the published article.

REFERENCES

[1] Fisher, S.K.; Novak, J.E.; Agranoff, B.W. Inositol and higher inositol phosphates in neural tissues: homeostasis, metabolism and functional significance. *J. Neurosci*., **2002**, *82*, 736–754.

[2] Michaelis, T.; Helms, G.; Merboldt, K.-D.; Hanicke, W., Bruhn, H.; Frahm, J. Identification of scyllo-inositol in proton NMR spectra of human brain *in vivo*. *NMR Biomed*., **1993**, *6*, 105–109.

[3] Seaquist, E.R.; Gruetter, R. Identification of a high concentration of *scyllo*-inositol in the brain of a healthy human subject using ^{1}H and ^{13}C NMR. *Magn. Reson. Med*., **1998**, *39*, 313–316.

[4] Shetty, H.U.; Schapiro, M.G.; Holloway, H.W.; Rapoport, S.I. Polyol profiles in Down syndrome: *myo*-inositol specifically is elevated in the cerebrospinal fluid. *J. Clin. Invest*., **1995**, *95*, 542–546.

[5] Clements Jr., R.S.; Diethelm, A.G. The metabolism of myo-inositol by the human kidney. *J. Laboratory Clin. Med*., **1979**, *93*, 210–219.

[6] Hauser, G.; Finelli, V.N. The biosynthesis of free and phosphatide myo-inositol from glucose in mammalian tissues. *J. Biol. Chem*., **1963**, *238*, 3224–3228.

[7] Kwon, H.M.; Yamauchi, A.; Uchida, S.; Preston, A.S.; Garcia-Perez, A.; Burg, M.B.; Handler, J.S. Cloning of the cDNA for a Na^{+}/*myo*-inositol cotransporter, a hypertonicity stress protein. *J. Biol. Chem*., **1992**, *267*, 6297–6301.

[8] Hager, K.; Hazama, A.; Kwon, H.M.; Loo, D.D.; Handler, J.S.; Wright, E.M. Kinetics and specificity of the renal Na+/*myo*-inositol cotransporter expressed in *Xenopus* oocytes. *J. Membr. Biol*., **1995**, *143*, 103–113.

[9] Coady, M.J.; Wallendorff, B.; Gagnon, D.G.; Lapointe, J.Y. Identification of a novel Na^{+}/*myo*-inositol cotransporter. *J. Biol. Chem*., **2002**, *277*, 35219–35224.

[10] Roll, P.; Massacrier, A.; Pereira, S.; Robaglia-Schlupp, A.; Cau, P.; Szepetowski, P. New human sodium/glucose cotransporter gene (*KST1*): identification, characterization, and mutation analysis in ICCA (infantile convulsions and choreoathetosis) and BFIC (benign familial infantile convulsions) families. *Gene*, **2002**, *285*, 141–148.

[11] Bourgeois, F.; Coady, M.J.; Lapointe, J.Y. Determination of transport stoichiometry for two cation-coupled *myo*-inositol cotransporters: SMIT2 and HMIT. *J. Physiol*., **2005**, *563*, 333–343.

[12] Uldry, M.; Ibberson, M.; Horisberger, J.D.; Chatton, J.Y.; Riederer, B.M.; Thorens, B. Identification of a mammalian H^{+}-*myo*-inositol symporter expressed predominantly in the brain. *EMBO J*., **2001**, *20*, 4467–4477.

[13] Thal, D.R.; Rüb, U.; Orantes, M.; Braak, H. Phases of Aβ-deposition in the human brain and its relevance for the development of AD. *Neurology*, **2002**, *58*, 1791–1800.

[14] Ostlund, Jr., R.E.; Seemayer, R.; Gupta, S.; Kimmel, R.; Ostlund, E.L.; Sherman, W.R. A stereospecific *myo*-inositol/D-chiro-inositol transporter in HepG2 liver cells. Identification with D-chiro-[3-^{3}H]inositol. *J. Biol. Chem*., **1996**, *271*, 10073–10078.

[15] Hakvoort, A.; Haselbach, M.; Galla, H.J. Active transport properties of porcine choroid plexus cells in culture. *Brain Res*., **1998**, *795*, 247–256.

[16] Bissonnette, P.; Coady, M.J.; Lapointe, J.Y. Expression of the sodium–*myo*-inositol cotransporter SMIT2 at the apical membrane of Madin-Darby canine kidney cells. *J. Physiol*., **2004**, *558*, 759–768.

[17] Aouameur, R.; Da Cal, S.; Bissonnette, P.; Coady, M.J.; Lapointe, J.Y. SMIT2 mediates all *myo*-inositol uptake in apical membranes of rat small intestine. *Am. J. Physiol. Gastrointest. Liver Physiol*., **2007**, *293*, G1300–G1307.

[18] Klaus, F.; Palmada, M.; Lindner, R.; Laufer, J.; Jeyaraj, S.; Lang, F.; Boehmer, C. Up-regulation of hypertonicity-activated *myo*-inositol transporter SMIT1 by the cell volume-sensitive protein kinase SGK1. *J. Physiol*., **2008**, *586*, 1539–1547.

[19] Lin, X.; Ma, L.; Fitzgerald, R.L.; Ostlund, Jr., R.E. Human sodium/inositol cotransporter 2 (SMIT2) transports inositols but not glucose in L6 cells. *Arch. Biochem. Biophys*., **2009**, *481*, 197–201.

[20] McLaurin, J.; Kierstead, M.E.; Brown, M.E.; Hawkes, C.A.; Lambermon, M.H.; Phinney, A.L.; Darabie, A.A.; Cousins, J.E.; French, J.E.; Lan, M.F.; Chen, F.; Wong, S.S.; Mount, H.T.; Fraser, P.E.; Westaway, D.; St. George-Hyslop, P. Cyclohexanehexol inhibitors of Abeta aggregation prevent and reverse Alzheimer phenotype in a mouse model. *Nat. Med*., **2006**, *12*, 801–808.

[21] Fenili, D.; Brown, M.; Rappaport, R.; McLaurin, J. Properties of *scyllo*-inositol as a therapeutic treatment of AD-like pathology. *J. Mol. Med*., **2007**, *85*, 603–611.

[22] www.clinicaltrials.gov. A service of the U.S. National Institutes of Health.

[23] Reizer, J.; Reizer, A.; Saier Jr., M.H. A functional superfamily of sodium/solute symporters. *Biochim. Biophys. Acta*, **1994**, *1197*, 133-166.

[24] Turk, E.; Wright, E.M. Membrane Topology Motifs in the SGLT Cotransporter Family. *J. Membr. Biol*., **1997**, *159*, 1-20.

[25] Abramson, J.; Paz, A.; Vartanian, A.S. Structures of the prokaryotic galactose transporter vSGLT and their implications on alternating access mechanisms in human SGLT1. In: Kramer, R.; Siegler, C (Editors). Membrane Transport Mechanism. 3D Structure and Beyond. Springer – Verlag, Berlin, Heidelberg, **2014**, pp. 59-78.

[26] White, S.H. Biophysical dissection of membrane proteins. *Nature*, **2009**, *459*, 344-346.

[27] Berman, H.M.; Westbrook, J.; Feng, Z.; Gilliland, G.; Bhat, T.N.; Weissig, H.; Shindyalov, I.N.; Bourne, P.E. The Protein Data Bank. *Nucl. Acids Res*., **2000**, *28*, 235-242.

[28] Faham, S.; Watanabe, A.; Besserer, G.M.; Cascio, D.; Specht, A.; Hirayama, B.A.; Wright, E.M.; Abramson, J. The crystal structure of a sodium galactose transporter reveals mechanistic insights into Na^{+}/sugar symport. *Science*, **2008**, *321*, 810-814.

[29] Biasini, M.; Bienert, S.; Waterhouse, A.; Arnold, K.; Studer, G.; Schmidt, T.; Kiefer, F.; Cassarino, T.G.; Bertoni, M.; Bordoli, L.; Schwede, T. SWISS-MODEL: modelling protein tertiary and quaternary structure using evolutionary information. *Nucl. Acids Res*., **2014**, *42*, W252-W258.

[30] Krieger, E.; Koraimann, G.; Vriend, G. Increasing the precision of comparative models with YASARA NOVA – a self-parameterizing force field. *Proteins*, **2002**, *47*, 393-402.

[31] Fenili, D.; Weng, Y.-Q.; Aubert, I.; Nitz, M.; McLaurin, J. Sodium/*myo*-inositol transporters: substrate transport requirements and regional brain expression in the TgCRND8 mouse model of amyloid pathology. *PLoS One*, **2011**, *6*, e24032.

[32] Jones, G.; Willett, P.; Glen, R.C.; Leach, A.R.; Taylor, R. Development and validation of a genetic algorithm for flexible docking. *J. Mol. Biol*., **1997**, *267*, 727-748.

Received: December 21, 2014 Revised: February 06, 2015 Accepted: February 12, 2015